Solid-State Dissimilar Joining of Ti-Fe with Nb and Cu Interlayers

Solid-state joining by vaporizing foil actuator welding; intermetallic compounds were successfully avoided with Nb and Cu interlayers

BY B. LIU, A. VIVEK, W. LIN, C. PROTHE, AND G. S. DAEHN

ABSTRACT

Direct titanium-steel joints are difficult to achieve because brittle Ti-Fe intermetallic compounds (IMCs) tend to form along the interface, especially at high temperatures. This problem can be prevented by inserting diffusion-inhibiting interlayers. In this work, a four-layer system, Ti-Nb-Cu-Fe, is investigated, where Nb and Cu are the interlayers. This combination is very stable against the formation of IMCs, as is evident by the phase diagrams of all the adjacent material pairs. Ti-Nb-Cu-Fe samples were made using vaporizing foil actuator welding (VFAW), a solid-state impact welding technique. The welding angles were assessed by using target plates with angled grooves, and the welding velocities by photonic Doppler velocimetry (PDV). All the welded samples were sectioned by electrical discharge machining (EDM) and examined metallographically. Welding windows were obtained by correlating the interfacial microstructures and the corresponding input parameters. One sample was subjected to heat treatment at 910°C for 24 h, furnace cooled, and then examined metallographically. The sample was found to be free of IMCs at all three interfaces. This proves Ti-Nb-Cu-Fe as a robust system for making IMC-free titanium-steel transition joints.

KEYWORDS

- Vaporizing Foil Actuator Welding (VFAW) • Welding Window
- Photonic Doppler Velocimetry • Grooved Target Plate • Ti-Fe Joining
- Cu/Nb Interlayer • Interdiffusion • Intermetallic Compounds
- Energy-Dispersive Spectroscopy

Introduction

Titanium-steel joints are of great interest for purposes of lightweighting and corrosion protection in aerospace and high-end automotive applications. However, it is difficult to effectively join titanium to steel using traditional fusion welding techniques, since these techniques involve high temperatures and melting, which cause brittle Ti-Fe intermetallic compounds (IMCs) to form along the interface — Fig. 1A (Refs. 1–4). In contrast, solid-state welding techniques, such as explosive welding (EXW) and friction stir welding, which involve much lower temperatures and little or no melting, can be used to produce nearly IMC-free Ti-Fe joints (Refs. 5, 6). Impact welding, in particular, takes place in a very short time and therefore involves a very short thermal cycle. This work employs vaporizing foil actuator welding (VFAW) (Ref. 7), which is a solid-state impact welding technique.

In impact welding, typically one member of the welding pair is held stationary, backed by a rigid anvil. The stationary piece is called the target. The other member, the flyer, is set at some standoff distance away from a target plate. The flyer and the target are often initially set up parallel to each other. During the welding event, the flyer is accelerated to a high speed and made to collide obliquely with the target. Given the right impact speed and angle, such an impact removes surface oxides and adsorbed gases from the faying surfaces and brings the two colliding members into atomistically intimate contact, thereby creating a solid-state weld (Ref. 8).

In VFAW, the flyer is propelled by electrically generated, rapidly expanding gas. The gas is derived from an aluminum-foil actuator in the shape of a 0.003-in.- (0.076-mm-) thick dogbone (Fig. 2), manufactured by electrical discharge machining (EDM). The ends of the actuator are connected to the output end of a capacitor bank, the characteristics of which are summarized in Table 1.

When the capacitor bank is discharged, it gives rise to a high current through the foil actuator and thus vaporizes the foil into rapidly expanding gas (Fig. 3), which propels the flyer to a high speed within about 10~20 μs. The peak flyer speed depends on a number of parameters but typically ranges from 400 to 1200 m/s. Vaporiz-

B. LIU (liu.2004@osu.edu), *A. VIVEK, and G. S. DAEHN are with The Ohio State University, Columbus, Ohio. W. LIN is with Pratt & Whitney, East Hartford, Conn. C. PROTHE is with Dynamic Materials, Mt. Braddock, Pa.*

Table 1 — Capacitor Bank Characteristic

Capacitance	426 μF
Inductance	100 nH
Resistance	10 mΩ
Maximum charging voltage	8.66 kV
Maximum charging energy	16 kJ
Short circuit current rise time	12 μs

ing foil actuator welding was developed in a laboratory setting and has been mainly used as a small-scale diagnostic tool, but its inventors are actively working on its adaptation in a manufacturing environment.

Critical parameters in impact welding include the angle and velocity of impact. The ranges of angles and velocities suitable for welding are called the welding window (Refs. 9, 10). In this work, impact angles are assessed by means of grooved target plates, and impact velocities by photonic Doppler velocimetry (PDV) (Refs. 11–13). Once the optimal processing parameters are determined, they can also be applied to other impact welding processes. In magnetic pulse welding (MPW), for example, the flyer plate can be initially set up at a desired angle relative to the target plate and then launched uniformly to collide with the target at that angle. The impact speed can be varied by controlling the input energy. In the case of EXW, the explosive loading and the standoff distance are tailored to vary both the impact speed and impact angle.

While solid-state welding techniques can prevent IMC formation during welding, they cannot prevent such formation during postwelding heat treatments or high-temperature applications, as heat treatment of the welded assembly may be needed to obtain desired material properties. In such cases, interlayers can be inserted between the IMC-forming pair to keep them physically separate. Appropriate interlayer materials and thicknesses must be selected such that they do not form IMCs of their own with neighboring materials and that they act as effective diffusion barriers. A particular four-layer system, Ti-Nb-Cu-Fe, was selected for this work, where Nb and Cu are the interlayers. Both Nb and Cu had already been used successfully as interlayers in joining dissimilar materials involving Fe or Ti (Refs. 14–18).

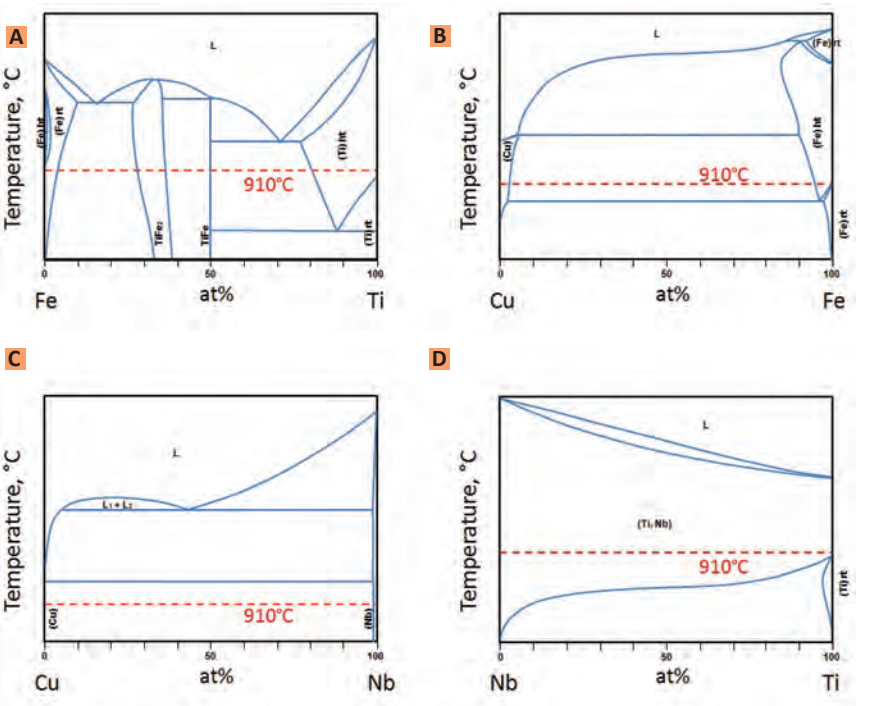

Fig. 1 — Binary phase diagrams of the following: A — Fe-Ti (Ref. 1); B — Cu-Fe (Ref. 2); C — Cu-Nb (Ref. 3); D — Nb-Ti (Ref. 4). Note that the latter three are all free of IMCs and complex phases. The heat treatment temperature, 910°C, is indicated by a red dashed line on each phase diagram. (Reprinted with permission of ASM International. All rights reserved. www.asminternational.org.*)*

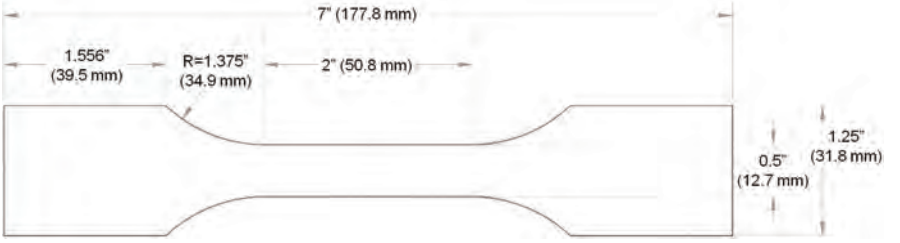

Fig. 2 — Schematic of 0.003-in.- (0.076-mm-) thick foil actuator used in VFAW.

Table 2 — Impact Velocities of arious Flyers and Input Energies

Input Energy (kJ)	Impact Velocity (m/s)		
	Cu→Fe	Nb→Cu	Ti→Nb
4.8	608	589[a]	620
6.4	661	642[a]	773
8.0	722	733	896

(a) = extrapolated

Experimental Methods

AISI 1018 steel target plates were cut to dimensions of 3 × 2 × 0.25 in. (76.2 × 50.8 × 6.4 mm) — Fig. 4. Six V-shaped grooves were machined into each target plate by EDM. Each groove had a different pitch angle: 8, 12, 16, 20, 24, and 28 deg, which covered the typical range of optimal impact angles. An extra groove was placed in the middle to accommodate the PDV hole, which was 3/16 in. (4.76 mm) in diameter. The target plates were sand blasted to remove the surface copper deposit from EDM and then manually

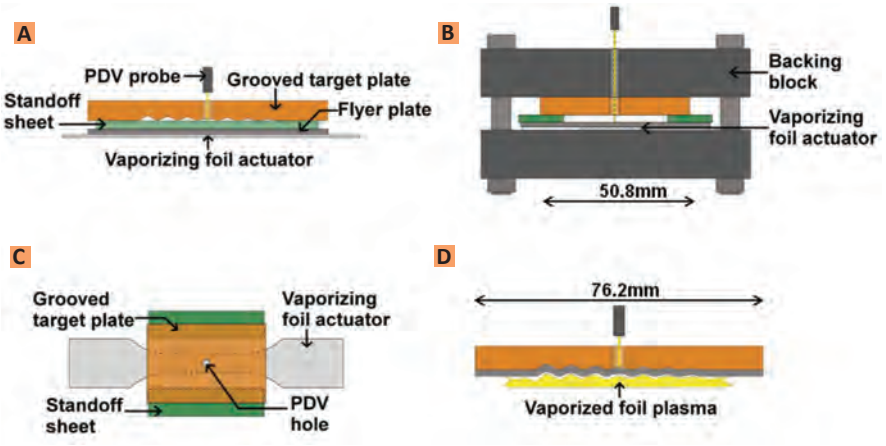

Fig. 3 — VFAW assembly: A — Side view; B — front view, including the backing blocks; C — top view; D — side view, during the welding event.

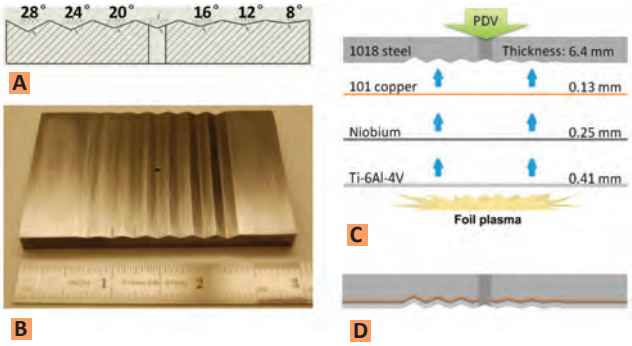

Fig. 4 — A — Schematic of the grooved portion of the target plate; B — manufactured grooved target plate; C — schematic of welding process, showing the order of three consecutive welding operations; D — schematic of welded sample.

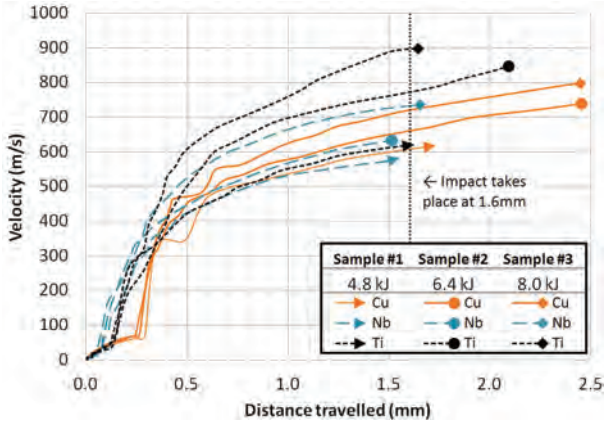

Fig. 5 — Velocity traces of Cu, Nb, and Ti flyers at 4.8, 6.4, and 6.0 kJ input energies.

filed to reduce surface roughness.

Before each VFAW operation, the faying surfaces of both the flyer and target were cleaned with acetone. The center of each flyer was crosshatched by grit paper to improve its reflectivity for the PDV probe laser. The standoff distance was 1.6 mm (0.063 in.) in all cases. The 0.005-in.- (0.13-mm-) thick Cu interlayer, 0.010-in.- (0.25-mm-) thick Nb interlayer, and 0.016-in.- (0.41-mm-) thick Ti-6Al-4V were welded to the steel target in that order, one on top of another, in three successive VFAW operations — Fig. 4. Thinner materials were chosen for the interlayers, while the thicker materials were used for the Fe and Ti bases. The exact flyer thicknesses were chosen based on materials that were readily available. For a given sample, the same input energy was used for all three welding operations. Three samples were prepared in this way, each representing a different input energy: 4.8, 6.4, and 8.0 kJ. Each energy value indicates the energy of the charged capacitor bank according to $E = 0.5\ CV^2$, where E is energy, C is capacitance, and V is charging voltage. It should be noted that only about 5–10% of the input energy is converted to the kinetic energy of the flyer (Refs. 12, 19). All the welded samples were then sectioned perpendicularly to the grooves by EDM, along the centerline of the foil actuator. The cross sections were examined metallographically.

In order to test the assembly's stability at high temperatures, the 8.0 kJ sample was heat treated at 910°C for 24 h and then furnace cooled. These conditions were selected to simulate a postweld heat treatment or a high-temperature application. The sample was then examined metallographically, both by optical microscopy and by energy-dispersive spectroscopy (EDS). Energy-dispersive spectroscopy data were taken in an FEI Quanta 200 scanning electron microscope, and composition analysis was done using standardless ZAF analysis of the intensity data using EDAX Genesis software. Accelerating voltage was 25 kV, spacing between points was about 3 µm, and dwell time at each point was 300 ms.

Results

The three four-layer samples all welded successfully in at least some of the grooves. The velocity traces are summarized in Fig. 5. Since the standoff distance is 1.6 mm, the velocity measured at 1.6 mm was taken to be the impact velocity (Table 2).

The samples were sectioned along the centerline, along the middle of the active area of the foil actuator. Standard mounting and polishing procedures were used. Six images were taken for each sample, one image for each angle, near the middle of the angled slope. A full array of weld interface morphologies was observed and summarized as follows — Fig. 6. They can be roughly categorized into no-weld, flat, small-wave, and wavy. By combining the speed and angle data with the interfacial microstructure, the preliminary welding windows of the three interfacing material pairs were obtained — Fig. 7.

The 16-deg groove of the 8-kJ sample had the best weld interfaces: the interfacial waves were well developed, indicating that sufficient material flow had taken place, and the interfaces were free of voids. This part of the sample was therefore chosen as a representative for the diffusion study. The corre-

sponding impact velocities can be found in Table 2. Line EDS was performed across all three interfaces, in two regions of the sample, in both as-welded and heat-treated conditions — Fig. 8. Significant interdiffusion was only detected at the Ti-Nb interface, in region 1, in the heat-treated sample.

Discussion

Impact Speed

In the cases of all three types of flyers used, higher input energies resulted in higher impact speeds (Table 2). At any given input energy, the Ti-6Al-4V flyer tended to be faster than the other two flyer materials. This difference may be due to the material's low density and relatively high stiffness, which confined the gas in a manner that is believed to improve the efficiency of the launch process.

The acceleration process in VFAW is compared to that in EXW, which is perhaps the most common industrial process for impact welding. In EXW, the explosives are typically loaded on the entire surface of the flyer plate. During the welding event, detonation is initiated at one end of the plate (or sometimes the middle of the plate) and a detonation front travels across the entire area of the plate. Large pressure is generated at the detonation front, which propels the flyer plate toward the target plate, and because the detonation front travels at some finite velocity, the flyer plate is collapsed onto the target plate gradually from one end to another. Thus, explosive energy is supplied continuously throughout the welding event, gradually across the length of the flyer plate. This is also how EXW is capable of producing very large clad sheets.

In VFAW, the acceleration event can be divided into three stages. First, when the capacitor bank is just discharged and current rises in the foil actuator, prior to the burst event, the flyer is propelled by electromagnetic forces. This stage corresponds to a gentle rise in velocity over about 7 to 10 μs. This rise is more significant with more conductive metals, such as copper. Second, at the burst event, a high-pressure pulse is generated that accelerates the flyer very sharply. Third, as the aluminum vapor from the foil burst reacts with oxygen exothermically, it continues to expand and propel the flyer plate for the rest of its flight.

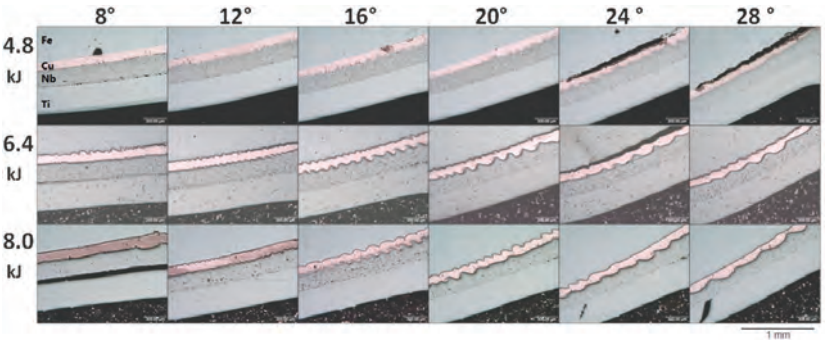

Fig. 6 — Weld interface morphologies from various collision angles and input energies.

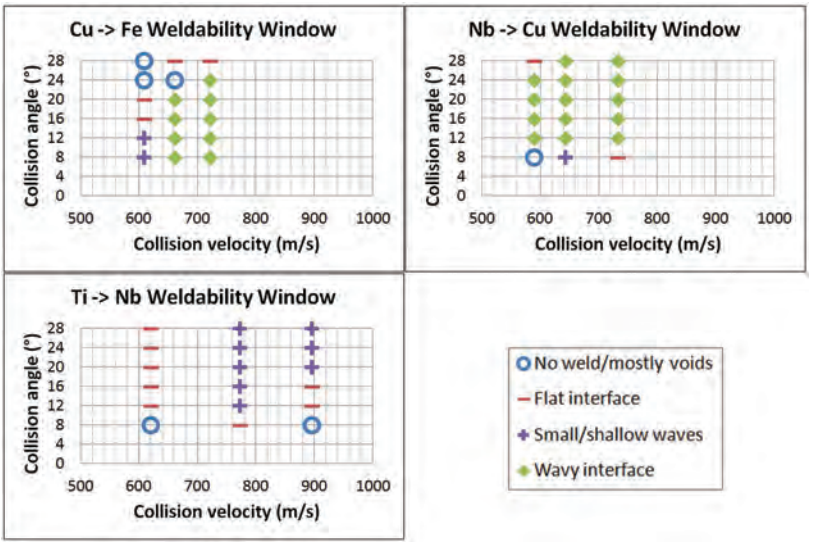

Fig. 7 — Preliminary welding windows.

The acceleration during the second stage is the most significant, by far, since this stage corresponds with the foil burst event. This burst event is assumed to take place simultaneously across the active area of the foil actuator, which is approximately a long, narrow rectangle. The flyer immediately above this active area is assumed to be launched uniformly. This assumption was supported by experiments that showed similar velocities at different points along the active length of the foil actuator (Ref. 20). In this work, only this area of the welded sample was used for analysis.

In some cases, the velocity trace was seen to extend beyond the initial point of impact, and the velocity was even found to continue to increase — Fig. 5. This is due to the propulsion by expanding gases, corresponding to the third stage of flyer acceleration. After the initial impact, which takes place at the top of the groove, the flyer continues to travel until it reaches the bottom of the groove, which was initially 2.76 mm away from the flyer plate. The recorded velocity trace, though, can terminate before the bottom of the groove is reached, if the flyer surface evolves in such a way that puts the probing laser out of alignment. In this work, the longest recorded flight was about 2.45 mm.

Whereas EXW's acceleration is continuous and gradual across the length of the weld area, VFAW's acceleration is instantaneous and uniform. Nonetheless, they both result in gradual, oblique impacts between the flyer and target plates. In EXW, this is achieved by gradual detonation across the flyer plate, and in VFAW, this is achieved by using an angled (grooved) target. Since the grooves are shallow,

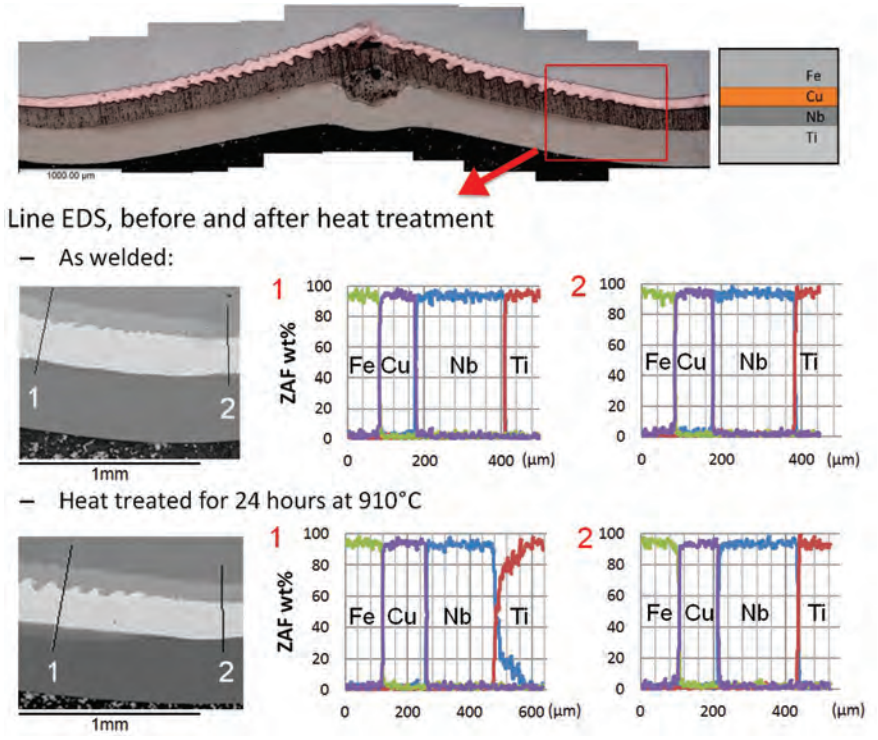

Fig. 8 — Line EDS in (1) welded region and (2) unwelded region of the 16-deg groove of the 8-kJ sample, both before and after heat treatment. The two SEM images on the left are backscatter-electron images.

the speed variation along the weld length was believed to be small. So although the acceleration processes in VFAW and in EXW are not entirely the same, their speed-angle impact conditions are believed to be sufficiently comparable.

Interfacial Morphology

Some of the welded interfaces exhibited wavy features — Fig. 6. A wavy interface is a typical feature, though not a requirement, of successful impact welds (Ref. 21). Factors that affect the tendency of wave formation include the hardnesses and densities of both members of the colliding material pair (Ref. 22). Softer and denser materials tend to weld more readily and have wider welding windows. The thicknesses of both members of the joining pair have also been suggested to affect the interfacial morphology (Ref. 23). This is consistent with what was observed in this work: the Cu and Nb are relatively dense and soft, and the Cu-Nb interface was found to weld and form wavy features most readily. On the other hand, the interface involving the high-strength, low-density Ti-6Al-4V had the lowest tendency to form wavy features in the range of angles and velocities investigated here.

Diffusion

In Fig. 8, region 1 was welded, as is evident by the interfacial morphology. Region 2 was not welded because it was positioned in a flat-impact area, and flat impacts do not result in successful impact welds. In both areas of the as-welded samples, no interdiffusion was observed and no IMCs were found, since the short time scale and low temperature of the welding process did not allow for diffusion to take place to any significant extent. The unwelded region of the heat-treated sample also showed no sign of diffusion since the unwelded interfaces were not atomistically intimate. Significant interdiffusion only took place in the heat-treated sample, in the welded region, at the Ti-Nb interface.

The EDS results show that all the IMC-forming pairs were kept physically apart and no IMCs were found at any of the interfaces, even after prolonged heat treatment. This confirms that the chosen interlayers are effective diffusion barriers. The binary phase diagrams (Fig. 1) (Refs. 1–4) of all the adjacent pairs in Ti-Nb-Cu-Fe shed light on why this might be the case: They are all free of intermetallics or complex phases at all compositions and temperatures. Furthermore, Cu-Fe and Nb-Cu are both mostly immiscible at 910°C. This is consistent with the fact that no diffusion was observed at these interfaces. On the other hand, Ti-Nb is fully miscible at 910°C, thus interdiffusion was observed at this interface, but since the diffusivity of Ti in Nb is low, the penetration of Ti into Nb is shallow. Based on pure Ti-Nb diffusion experiments, the impurity diffusivity of Nb in Ti is estimated to be $2.87*10^{-10}$ cm^2/s (Ref. 24), whereas that of Ti in Nb is only about $8.37*10^{-18}$ cm^2/s (Ref. 25). In other words, the diffusivity of Ti into Nb is lower than that of Nb into Ti by some eight degrees of magnitude, so Ti could not easily diffuse across the Nb layer to form IMCs with Cu. Therefore, even though diffusion did take place, the interlayers were still effective in keeping the IMC-forming pairs physically separated.

It should be noted that the diffusivity values stated above are based on experiments done with pure systems, whereas the system at hand contains alloys. At the heat treatment temperature of 910°C, pure Ti has a body-centered cubic (BCC) structure, but Ti-6Al-4V has a BCC + HCP (hexagonal close packed) structure. In other words, the available diffusivity data do not fully represent the system at hand, but they do provide estimation and indicate a strong trend that the diffusion of Ti into Nb is very low.

Mechanical Properties

In the case of very drastic temperature fluctuations, the mismatch in the coefficients of thermal expansion among the four layers of materials may give rise to internal stresses that may be a concern. In the present work, the bonds were at least strong enough to survive the heat treatment cycle where T = 885°C. The regions immediately adjacent to the interfaces are generally hardened due to shock hardening, work hardening, and grain refinement. The postweld heat treatment reverses these

hardening effects to some extent by annealing (Ref. 6).

Conclusion

- Ti-Nb-Cu-Fe samples were manufactured by vaporizing foil actuator welding using three different foil vaporization energies: 4.8, 6.4, and 8.0 kJ, which provided impact speeds in the approximate range of 600 to 900 m/s for this geometry.
- Preliminary impact welding windows of all the neighboring material pairs were obtained. This information is also relevant in large-scale impact welding production processes, for the purpose of manufacturing lightweight or corrosion-protected structures.
- At all three input energies, 0.016-in.-(0.41-mm-) thick Ti-6Al-4V tended to travel the fastest among the three flyer materials used in this work.
- The Nb-Cu interface tended to weld and form wavy features most readily.
- Ti-Nb-Cu-Fe proved to be stable against the formation of IMCs even after prolonged heat treatment (910°C for 24 h) and is therefore a suitable combination for Ti-Fe joining where postwelding heat treatments or high-temperature applications are required.

Acknowledgment

This work was supported by the sponsorship of Pratt & Whitney, as part of the Industry & University Cooperative Research Program of the National Science Foundation. Special thanks also go to Dynamic Materials for sharing its knowledge on impact welding, and to Dr. John Morral of The Ohio State University for sharing his knowledge on diffusion.

References

1. Ohtani, H., et al. 2006. Fe-Ti phase diagram. ASM Alloy Phase Diagrams Database, P. Villars, editor-in-chief; H. Okamoto and K. Cenzual, section editors; *www1.asminternational.org/AsmEnterprise/APD*. Materials Park, Ohio: ASM International.

2. Amara, S. E., et al. 1999. Cu-Fe Phase Diagram. ASM Alloy Phase Diagrams Database, P. Villars, editor-in-chief; H. Okamoto and K. Cenzual, section editors; *www1.asminternational.org/AsmEnterprise/APD*. Materials Park, Ohio: ASM International.

3. Okamoto, H., et al. 1991. Cu-Nb Phase Diagram. ASM Alloy Phase Diagrams Database, P. Villars, editor-in-chief; H. Okamoto and K. Cenzual, section editors; *www1.asminternational.org/AsmEnterprise/APD*. Materials Park, Ohio: ASM International.

4. Okamoto, H., et al. 2002. Nb-Ti Phase Diagram. ASM Alloy Phase Diagrams Database, P. Villars, editor-in-chief; H. Okamoto and K. Cenzual, section editors; *www1.asminternational.org/AsmEnterprise/APD*. Materials Park, Ohio: ASM International.

5. Dey, H. C., Ashfaq, M., Bhaduri, A. K., and Prasad Rao, K. 2009. Joining of titanium to 304L stainless steel by friction welding. *Journal of Materials Processing Technology* 209(18): 5862–5870.

6. Inal, O. T., Szecket, A., and Vigueras, D. J. 1985. Explosive welding of Ti–6Al–4V to mild-steel substrates. *Journal of Vacuum Science & Technology A* 3(6): 2605–2609.

7. Vivek, A., Hansen, S. R., Liu, B. C., and Daehn, G. S. 2013. Vaporizing foil actuator: A tool for collision welding. *Journal of Materials Processing Technology*.

8. Akbari Mousavi, A. A., and Al-Hassani, S. T. S. 2005. Numerical and experimental studies of the mechanism of the wavy interface formations in explosive/impact welding. *Journal of the Mechanics and Physics of Solids* 53(11): 2501–2528.

9. Akbari Mousavi, S. A. A., and Farhadi Sartangi, P. 2009. Experimental investigation of explosive welding of cp titanium/AISI 304 stainless steel. *Materials & Design* 30(3): 459–468.

10. Jaramillo, D., Szecket, A., and Inal, O. T. 1987. On the transition from a waveless to a wavy interface in explosive welding. *Materials Science and Engineering* 91: 217–222.

11. Strand, O. T., Goosman, D. R., Martinez, C., Whitworth, T. L., and Kuhlow, W. W. 2006. Compact system for high-speed velocimetry using heterodyne techniques. *Review of Scientific Instruments* 77(8): 083108.

12. Vivek, A., Hansen, S. R., and Daehn, G. S. 2014. High strain rate metalworking with vaporizing foil actuator: Control of flyer velocity by varying input energy and foil thickness. *Review of Scientific Instruments* 85(7): 075101.

13. Vivek, A., Liu, B. C., Hansen, S. R., and Daehn, G. S. 2014. Accessing collision welding process window for titanium/copper welds with vaporizing foil actuators and grooved targets. *Journal of Materials Processing Technology* 214(8): 1583–1589.

14. Kuo, M. 1994. Dissimilar friction welding of titanium alloys to Alloy 718. *Dissertation Abstracts International* 54(8): 145.

15. Cola, M. J., Lyons, M. B., Teter, D. F., and Gentzlinger, R. C. 1999. Dissimilar metal joints for the APT superconducting cavity's cryogenic plumbing systems. *Proceedings of the 1999 InParticle Accelerator Conference.* Vol. 2, pp. 962–964. IEEE.

16. Kundu, S., Ghosh, M., Laik, A., Bhanumurthy, K., Kale, G. B., and Chatterjee, S. 2005. Diffusion bonding of commercially pure titanium to 304 stainless steel using copper interlayer. *Materials Science and Engineering: A* 407(1): 154–160.

17. Ha, Jong Su, and Sun, Ig Hong. Design of high strength Cu alloy interlayer for mechanical bonding Ti to steel and characterization of their tri-layered clad. *Materials & Design* 51 (2013): 293-299.

18. Kundu, S., and Chatterjee, S. 2010. Evolution of interface microstructure and mechanical properties of titanium/304 stainless steel diffusion bonded joint using Nb interlayer. *ISIJ International* 50(10): 1460–1465.

19. Vivek, A., Taber, G. A., Johnson, J. R., Woodward, S. T., and Daehn, G. S. 2013. Electrically driven plasma via vaporization of metallic conductors: A tool for impulse metal working. *Journal of xMaterials Processing Technology* 213(8): 1311–1326.

20. Hansen, S. R., Vivek, A., and Daehn, G. S. 2014. Control of velocity, driving pressure, and planarity during flyer launch with vaporizing foil actuator. *Proceedings of the 6th International Conference on High Speed Forming,* Daejeon, Korea. *http://hdl.handle.net/2003/33476*.

21. Szecket, A., Inal, O. T., Vigueras, D. J., and Rocco, J. 1985. A wavy versus straight interface in the explosive welding of aluminum to steel. *Journal of Vacuum Science & Technology A* 3(6): 2588–2593.

22. Cowan, G. R., Bergmann, O. R., and Holtzman, A. H. 1971. Mechanism of bond zone wave formation in explosion-clad metals. *Metallurgical and Materials Transactions B* 2(11): 3145–3155.

23. Ben-Artzy, A., Stern, A., Frage, N., Shribman, V., and Sadot, O. 2010. Wave formation mechanism in magnetic pulse welding. *International Journal of Impact Engineering* 37(4): 397–404.

24. Peart, R. F., and D. H. Tomlin. 1962. Diffusion of solute elements in beta-titanium. *Acta Metallurgica* 10(2): 123–134.

25. Pelleg, J. 1970. Diffusion of 44Ti into niobium single crystals. *Philosophical Magazine* 21, No. 172: 735–742.